HHS Public Access

Author manuscript

*Mol Imaging Biol*. Author manuscript; available in PMC 2017 April 01.

Published in final edited form as:

*Mol Imaging Biol*. 2016 April ; 18(2): 219–231. doi:10.1007/s11307-015-0885-x.

# Evaluation of CAIX and CAXII Expression in Breast Cancer at Varied $O_2$ Levels: CAIX is the Superior Surrogate Imaging Biomarker of Tumor Hypoxia

**Narges K. Tafreshi**[1], **Mark C. Lloyd**[2], **Joshua B. Proemsey**[2], **Marilyn M. Bui**[2,3,4], **Jongphil Kim**[5], **Robert J. Gillies**[1], and **David L. Morse**[1]

[1]Department of Cancer Imaging & Metabolism, H. Lee Moffitt Cancer Center and Research Institute, Tampa, FL, 33612, USA

[2]Analytic Microscopy Core Facility, H. Lee Moffitt Cancer Center and Research Institute, Tampa, FL, 33612, USA

[3]Breast Program, H. Lee Moffitt Cancer Center and Research Institute, Tampa, FL, 33612, USA

[4]Department of Anatomic Pathology, H. Lee Moffitt Cancer Center and Research Institute, Tampa, FL, 33612, USA

[5]Department of Biostatistics, H. Lee Moffitt Cancer Center and Research Institute, Tampa, FL, 33612, USA

## Abstract

**Purpose—**Hypoxia is commonly observed in regions of primary tumors and metastases, and is associated with resistance to treatment, more aggressive tumor phenotypes and poor prognosis. Reliable and validated imaging biomarkers of hypoxia are needed for pre-clinical studies and clinical use. Expression of cell-surface carbonic anhydrases IX and XII (CAIX and CAXII) in tumor cells has been associated with tumor hypoxia. CAIX and CAXII specific antibodies conjugated to fluorescent dye were evaluated for the non-invasive detection of hypoxia *in vivo*.

**Procedures—**Human breast cancer cell lines (MCF10A, DCIS, MCF7, ZR-75.1 and MDA-mb231) were characterized for CAIX and CAXII expression by real-time RT-PCR and immunocytochemistry (ICC) under normoxic and hypoxic conditions. Immunohistochemical (IHC) staining of CAIX, CAXII and the commercially available exogenous hypoxia marker, pimonidazole, was performed using sections of ZR-75.1 and MDA-mb-231 orthotopic breast cancer xenograft tumors from nude mice. *In vivo* fluorescence imaging of ZR-75.1 tumors in animals housed at varied levels of oxygen was used to quantify the relative uptake of the CAIX and CAXII agents and a commercially available sulfonamide-based agent. Corresponding tumor sections were IHC stained for CAIX, CAXII and pimonidazole.

**Results—**CAIX mRNA expression was significantly higher ($p<0.05$) in hypoxia for all cell lines, which was in agreement with protein expression by ICC. CAXII expression was mixed, with a modest hypoxia-related increase in two cell lines ($p<0.05$) and no change in others. Quantified

*Correspondence to:* David Morse; david.morse@moffitt.org.

*Conflict of Interest*. All authors declare that they have no competing interest.

IHC staining of ZR-75.1 and MDA-mb-231 tumor sections showed that CAIX and CAXII expression was elevated in regions with pimonidazole staining, but CAXII levels were lower than CAIX. Tumor uptake of the CAIX targeted agent, and IHC staining of CAIX and pimonidazole in corresponding tumor sections were correlated, and co-registered, and shown to be significantly elevated by level of oxygenation ($p<0.001$): hypoxia>normoxia>hyperoxia. However, the CAXII and sulfonamide agents were not significantly correlated with hypoxia.

**Conclusion—**These studies suggest that the fluorescently labeled CAIX-specific agent is a more robust indicator of hypoxia *in vivo* compared to the CAXII-specific agent or the agent specific to the CA active site.

### Keywords

Breast cancer; Carbonic anhydrase IX; Carbonic anhydrase XII; Targeted agents; Non-invasive imaging of hypoxia

## Introduction

Because of perfusion deficits, solid tumors have heterogeneous regions of hypoxia (reduced $pO_2$) [1]. Additionally, it has been reported that the altered tumor metabolism can also contribute to tumor hypoxia [2, 3]. In multiple cancer types, hypoxia has been shown to be associated with cancer initiation and progression, with resistance to treatment with radiation and cytotoxic chemotherapeutics [4], and to have clinical relevance as a prognostic marker of poor survival [5, 6]. The generally negative sequelae of tumor hypoxia have been a rationale for the development of a new family of hypoxia-activated pro-drugs [7]. These properties of tumor hypoxia make relevant the ability to detect hypoxic regions which can help decide which patients could be benefit from adjunctive anti-hypoxia therapy as well as to monitor therapy response [8].

An ideal method for assessment of tumor hypoxia should be clinically safe, readily available, minimally invasive with low exposure to radiation, high resolution and easy to use [9]. Techniques for measuring oxygen can be divided into direct measurement such as needle electrodes and indirect measurements of oxygen [8, 10]. Direct tumor $pO_2$ measurement by microelectrode has been used in clinical studies and is considered a reference standard [10]. However, use of this method is restricted by the difficulty of accessing tumors, cost, sampling error, invasiveness, inter-observer variability [11], failure to distinguish necrosis from hypoxia [12] and difficulty in calibration [8].

Detection of hypoxia can be provided by indirect measurements [13], *e.g.*, immunohistochemical (IHC) analyses of tumor biopsies based on endogenous hypoxia-associated protein expression such as HIF-1α [14] and carbonic anhydrase isoform 9, CAIX [15, 16], or exogenous markers such as pimonidazole and EF5 (2-nitroimidazole) that are preferentially trapped in hypoxic cells [17, 18]. Clinically, positron emission tomography (PET) probes based on 2-nitroimidazoles have been developed, such as $^{18}$F-misonidazole, $^{18}$F-HX4, $^{18}$F-FAZA and $^{18}$F-EF5 [reviewed by [19]]. These probes measure bioreductive pathway activation under hypoxia, yet are sometimes limited by small dynamic

range and hence, poor tumor-to-background ratios. In addition, non-oxygen-dependent metabolism can lead to non-specific signal generated by these probes [20].

Intrinsic hypoxic markers can be distinguished from 2-nitroimidazole-based agents in that they are sensitive to biological hypoxia, *i.e.*, the response of cells to a hypoxic environment. While this can be variable, they are advantageous in that they may be more predictive of outcome [21]. Hence, it is desirable to complement the *ex vivo* analysis of intrinsic targets with a molecular imaging approach based on selective agents to accessible proteins that are over-expressed at sites of hypoxia.

Hypoxia inducible factor 1 (HIF-1) is stabilized in response to hypoxia, allowing for binding to the hypoxia response element (HRE) in the promoter region of a large number of genes involved in cancer progression and tumor growth [22]. One of the most investigated targets of HIF-1α is CAIX [16]. CAIX is a transmembrane protein that catalyzes the reversible hydration of carbon dioxide, and its high expression has been independently associated with poor prognosis in a growing number of tumor types (for reviews, see [23, 24]), making it an attractive target for diagnostic non-invasive imaging, a potential biomarker of treatment response and an endogenous marker of hypoxia (reviewed by [25]).

Carbonic anhydrase 12 (CAXII) is another membrane-bound carbonic anhydrase that has been shown to be over-expressed or co-expressed with CAIX in several tumor types, including breast cancer [26–28]. While CAIX is only rarely expressed in normal tissues, CAXII is present in many normal tissues. CAXII expression can also be induced by hypoxia, but the underlying molecular mechanism remains unknown [16, 29]. The *CA12* gene promoter does not contain an HRE that corresponds to the HRE of *CA9*. However, the upstream region of the *CA12* gene does possesses several putative HRE sequences [16], but their functionality has not been documented. Both CAIX and CAXII isoenzymes have attracted attention, not only as functional components of tumor physiology but also as tumor biomarkers and potential therapeutic targets [27, 30]. A radiolabeled CAIX antibody ($^{124}$I-cG250) that is specific against CAIX for clear cell renal cell carcinoma (ccRCC) with constitutively expressed CAIX has been developed for diagnosis of ccRCC and has shown excellent sensitivity, specificity, and positive and negative predictive value in patients with ccRCC [31, 32].

To study the feasibility of using CAIX and/or CAXII as surrogate markers of tumor hypoxia, their expression patterns were evaluated *in vitro*, *ex vivo* and *in vivo* using a set of breast cancer cell lines and xenograft tumors in the context of both normoxia and hypoxia. Previously, we had developed CAIX- or CAXII-specific monoclonal antibodies conjugated to a near-infrared fluorescent (NIRF) dye excited at 680 nm (CA9Ab-680 and CA12Ab-680, respectively) as *in vivo* imaging probes [27]. Additionally, a commercially available sulfonamide-based fluorescent agent that binds to extracellular carbonic anhydrases (HypoxiSense 680, Perkin-Elmer) was also evaluated [33]. To study the feasibility of using these as *in vivo* imaging probes of hypoxia, they were injected intravenously into animals bearing xenograft tumors housed in normoxic, hypoxic and hyperoxic conditions.

## Materials and Methods

### Cell Culture

MDA-mb-231 and ZR-75.1 cells were grown in RPMI 1640; MCF-10A and DCIS cells were grown in Mammary Epithelial Cell Growth Medium (MEGM, Lonza, Allendale, SC) containing 10 % fetal bovine serum (Life Technologies, Gaithersburg, MD), 0.03 %$_{L}$-glutamine, 100 units/ml penicillin and 100 μg/ml streptomycin, and cell cultures were grown in 5 % $CO_2$ at 37 °C. The cell lines were obtained from American Type Culture Collection (ATCC), expanded for two passages, and cryopreserved. All experiments were performed using cells of passage number less than 25. Cell morphology was monitored by microscopy and cells were confirmed to maintain their morphology throughout the study. Also, cells were authenticated as free of mycoplasma by testing at ATCC.

In cyto hypoxia response experiments were conducted by incubating cells for approximately 20 h in <2 % $O_2$, 93 % $N_2$ and 5 % $CO_2$ (hypoxia) in a hypoxia chamber (BioSpherix, Xvivo system, G300C, NY) or 20 % $O_2$, 75 % $N_2$ and 5 % $CO_2$ (normoxia).

### Quantitative Real-Time RT-PCR (qRT-PCR)

RNA was extracted from each clone using an RNA extraction kit (Qiagen, Valencia, CA). *CA9* and *CA12* specific primer sets were designed using Gene Runner Software for Windows version 3.05. The *CA9* primers were designed to specifically detect the longer transcript. This is important for studies related to hypoxia-related expression of *CA9*, where the presence of the alternatively spliced variant is hypoxia-independent and can provide a false-positive signal [34]: forward-CA9, 5′-TTGAATGGGCGAGTGATTGAG-3′ and reverse-CA9 5′-CAGGGCTAGGATGTCACCAG-3′; and forward-CA12, 5′-CTGGCATCATGTATTTAGGGGC-3′ and reverse-CA12, 5′-GAGTTGCGCCTGTCAGAAAC-3′. β-actin was used for normalization as described in our previous study [35].

### Conjugation of Antibodies to Dye and Fluorescence Microscopy Studies

Anti-human CAIX monoclonal antibody (mAb) (Clone 303123, R&D systems, Minneapolis, MN) and CAXII mAb (Clone 315602, R&D system) were conjugated to VivoTag-S 680 (Perkin-Elmer, Cambridge, MA) as described in our previous study [27]. The immunogen for the CAIX and CAXII antibodies are rhCA9; accession # NP_001207; aa 59 – 414, and rhCA12; accession # NP_001209; aa 25 – 291, respectively, and both correspond to the extracellular domain at the N-terminus. Conjugates were purified with Sephadex G25 columns (Roche) and eluted into sterile tubes. Protein (A280) and dye (A680) absorbance was determined using an ND-1000 spectrophotometer (NanoDrop, Wilmington, DE) and used to confirm the number of fluorophore molecules conjugated to each antibody molecule. The conjugates were termed CA9Ab-680 and CA12Ab-680, respectively.

### Immunocytochemistry and Fluorescence Microscopy

Four hundred thousand cells were plated onto glass coverslips at the bottom of six-well plate and incubated in normoxic and hypoxic conditions as described above under “Cell Culture”

and were fixed with a 1:1 mixture of cold methanol, air-dried, block and stained with CA9Ab-680 or CA12Ab-680, wheat germ agglutinin (WGA), Oregon Green 488 conjugate (Invitrogen) and 4′,6-diamidino-2-phenylindole (DAPI) as described previously [27].

## Tumor Xenograft Studies and in vivo Fluorescence Imaging

All procedures were carried out in compliance with the Guide for the Care and Use of Laboratory Animal Resources (2012), National Research Council, and approved by the Institutional Animal Care and Use Committee, University of South Florida.

To study the CA9Ab-680, CA12Ab-680 and HypoxiSense 680 (Perkin-Elmer) imaging probes *in vivo*, female *nu/nu* mice 6–8 weeks old, average weight of 23 g (Harlan Sprague Dawley, Inc., Indianapolis, IN) were implanted subcutaneously (s.c.) with a 60-day estrogen-release pellet containing 0.72 mg of estradiol (Innovative Research of America, Sarasota, FL) under 3 to 4 % isoflurane anesthesia. Two days after implantation, $5\times10^6$ ZR-75.1 cells were injected in the right mammary fat pad (MFP). Tumor volume was determined with calipers using the formula: volume=(−length×width$^2$)/2. Imaging studies were performed for three groups of animals with tumors in varied levels of oxygenation: hypoxia, normoxia and hyperoxia [7, 33, 36]:

Tumor hypoxia was induced by placing animals in an induction chamber with a continuous flow of 5 l/min of 7 % oxygen (residual $N_2$) for 2 h. Then, 50 μg of the CA9Ab-680 or CA12Ab-680 imaging probes, or 2 nmol of the HypoxiSense 680 imaging probe per manufacturer's protocol, were i.v. injected into each mouse. Animals were re-exposed to 7 % oxygen for an additional 5 h.

To increase oxygenation, animals were i.v. injected with 500 mg/kg of nicotinamide (Sigma-Aldrich) and then were placed in an induction chamber with a continuous flow of 5 l/min of carbogen (95 % O2, 5 % CO2, NTG Sol) for 2 h, followed by i.v. injections of probes and re-expose to carbogen for additional 5 h as described above [36]. For normoxic conditions, animals were housed in standard caging breathing air for 2 h following agent administration and imaging 5 h post-injection. The same method has been used by Dubois and colleague to evaluate fluorescent labeled sulfonamide probes [33].

Animals were imaged 5 h post agent administration using the Optix MX3 (ART Advanced Research Technologies Inc., Montreal, Canada) imaging system. Fluorescence images were acquired with raster scan points 1 mm apart (scan resolution) using a 670-nm pulsed laser diode with 40 MHz frequency and a 12 ns time window per raster point. According to the manufacturer, the excitation maxima of unconjugated VivoTag-S$^{™}$680 dye is 673±5 nm and the emission maxima is 691±5. Autofluorescence background was subtracted by determining the mean tumor fluorescence signal in normalized counts prior to injection. Images were analyzed using Optix-MX3 Optiview Software (version 2.01.00) and normalized count values were obtained within a circular region of interest (ROI) on the images. Fluorescence tomographic images were generated *via* time-domain optical imaging [37] using the Optix MX-3 imager and Optiview Software. Fluorescence lifetime gating was conducted using gating for peak Vivo-Tag 680 dye fluorescence lifetime of approximately

1.2 ns and the Optiview Software was used for 3D reconstruction based on time-domain data as described by Kumar *et al.* [37].

## Ex vivo Microscopy Studies and Immunohistochemistry Analysis

To assess hypoxia *ex vivo*, tumor-bearing mice were injected *via* the tail vein with 60 mg/Kg of the hypoxia cell marker pimonidazole hydrochloride (1-[(2-hydroxy-3-piperidinyl) propyl]-2-nitroimidazole hydrochloride (Natural Pharmacia International Inc., Burlington, MA)) 30 min before *in vivo* imaging (above) followed by euthanasia. To assess tumor perfusion, the *in vivo* DNA binding dye Hoechst 33342 (10 mg/Kg, Invitrogen) was i.v. injected 1 min before euthanizing the animals. Excised tumors were cut into two parts; one half of each excised tumor was fixed in formalin and embedded in paraffin, the other half was placed in Tissue-Tek Optical Cutting Temperature (OCT) cryoembedding media (Sakura Finetek, Torrance, CA) and snap frozen in liquid nitrogen until cryosectioned into 4-μm sections which were stored at −80 °C until staining for microscopic studies.

For confocal fluorescence microscopy studies, frozen sections were thawed and fixed in cold acetone (4 °C) for 10 min followed by rinsing and incubation overnight at 4 °C with mouse monoclonal anti-pimonidazole antibody (clone 4.3.11.3) (Natural Pharmacia International Inc., Burlington, MA) diluted 1:10 in PBS containing 0.1 % bovine serum albumin and 0.1 % Tween 20. The sections were then incubated with goat anti-mouse Alexa flour-488 secondary antibody, 1:3,000 diluted in phosphate buffered saline Tween-20 (PBST; Invitrogen, Grand Island, NY) for 1 h. Sections were then stained for CAIX or CAXII using our fluorescent probes (CA9Ab-680 or CA12Ab-680) as described for immunocytochemistry (ICC) and confocal fluorescence micrographs acquired with an SP5 laser scanning confocal microscope with Acousto-Optical Beam Splitter (AOBS, Leica Microsystems GmbH, Wetzlar, Germany). Hoechst nuclear staining was performed *in vivo* prior to euthanization as described above. ROIs within the micrographs were drawn that included necrotic areas that had cells without nuclear staining or viable areas that had cells with nuclear staining. Pixel-by-pixel binning distribution analyses were performed using LAS AF software version 1.6.0 build 1016 (Leica Microsystems GmbH, Wetzlar, Germany) for quantification of each ROI. Regional colocalization results were plotted and reported as overlap coefficients using the colocalization analysis module within the LAS AF software.

Slides were IHC stained using a Ventana Discovery XT automated system and OmniMap anti-mouse HRP detection system (Ventana Medical Systems, Tucson, AZ) as per manufacturer's protocol. Formalin-fixed sections (5 μm) were stained with a 1:500 dilution of anti-CAIX rabbit polyclonal antibody (abcam, Boston, MA), a 1:500 dilution of anti-CAXII rabbit antibody (Prestige Antibodies Powered by Atlas Antibodies, Sigma-Aldrich) or a 1:50 dilution of the same monoclonal anti-pimonidazole antibody, described above. A light hematoxylin nuclear staining was also performed as a counter-stain.

The Aperio ScanScope XT digital slide scanner (Aperio, CA) was used for scanning the slides at ×20 magnification. The whole slide CAIX and CAXII images were sub-segmented into blocks of superpixels (5×5 pixels) using Definiens Developer v1.2. For each stained tumor section, pattern recognition software was trained to identify and classify necrotic and viable tumor regions based on the nuclear staining pattern with quality control provided by a

board certified pathologist (Dr. Bui). The training was completed by choosing 20 regions which were identified by Dr. Bui as viable (10) or necrotic (10). The Definiens random forest algorithm was then capable of computationally completing the classification of either viable or necrotic tissue. Finally, the pathologist reviewed and confirmed the training and classification was accurate. Next, pixel-by-pixel staining intensities of CAIX and CAXII were quantified in regions of viable tumor and analyzed in relation to spatial distances from areas of necrosis. The distance in pixels was calculated from the center of all super pixels classified as viable tumor to the center of the nearest object classified as necrosis. The shortest straight line determined the minimum distance from tumor to necrosis. To provide a graphic representation comparing all of the distributions within a slide, three separate classifications for the necrosis distance were created: near necrosis, medium distance to necrosis and far from necrosis. “Near necrosis” included all of the superpixel objects within 400 pixels, “medium distance” included objects between 401 and 900 pixels and “far from necrosis” included hypoxic units greater than 901 pixels from the necrosis. Every 2 pixels are approximately 1 μm (0.502 μm/pixel).

For measuring the staining intensity in hypoxia, normoxia and hyper-$O_2$, immunopositivity of each biomarker was quantitatively scored using commercial algorithms from the Positive Pixel Count v9 Aperio Toolbox®. The staining intensity for strong (3+), moderate (2+), weak (1+) and negative (0) pixels were thresholded by the 0-255 8-bit dynamic range value (220; 175; 100; respectively). The algorithm was optimized for this study by a board-certified pathologist and applied to the entire slide’s digital image to determine the number and percentages of pixels expressing each intensity subset.

### Statistics

Data are represented as mean±standard deviation (S.D.). All statistical analyses were performed using SAS version 9.3 (Cary, NC), Matlab version 7.9.0 (Natick, MA), and GraphPad Prism version 5.01. A one-way ANOVA and the two-sided Tukey-Cramer 95 % simultaneous confidence intervals were used to determine significance among three independent groups, *i.e.*, normoxia, hypoxia and hyperoxia. The critical point for the Tukey-Cramer simultaneous confidence intervals and the corresponding *p* values were computed by the method of Kim [38]. For comparison of multiple groups, a *p* value of less than 0.025 was considered statistically significant, otherwise a *p* value of $<0.05$ was considered significant.

## Results

### In vitro Analysis of Hypoxia-related CA9 and CA12 mRNA Expression

In order to determine whether *CA9* or *CA12* expression differed by incubation in normoxic *vs*. hypoxic conditions, the mRNA levels of these genes were determined in a set of breast cancer cell lines (MCF-10A, DCIS, MCF-7, ZR-75.1 and MDA-mb-231) cultured in normoxic and hypoxic conditions using qRT-PCR. In normoxia, *CA9* mRNA was detectable in all five cell lines in normoxia, but at significantly lower levels compared to hypoxia ($p<0.05$) (Fig. 1). Normoxic expression of *CA9* was lowest in MCF-7 and ZR-75.1 cells and highest in the pre-neoplastic MCF-10A and pre-malignant DCIS cells. In comparison, *CA12* had higher levels of expression in normoxia compared to *CA9* in every case, which were

comparable to *CA9* levels in hypoxia or higher, and had only a slight, but significant ($p<0.05$) induction by hypoxia in two cell lines: MCF-10A and ZR-75.1 [39].

### In vitro Analysis of Hypoxia-Related CAIX and CAXII Protein Expression

We have previously developed monoclonal antibody-based CAIX and CAXII targeted NIRF molecular imaging probes (CA9Ab-680 and CA12Ab-680) for the non-invasive detection of breast cancer lymph node (LN) metastases and the high selectivity of the probes was confirmed *in vitro* and *in vivo* [24]. Here, to investigate the potential of using these probes to image biological hypoxia, we used them to detect CAIX and CAXII protein in cells cultured in hypoxic and normoxic conditions. The same cell lines and conditions reported above to determine mRNA expression were used. They were fixed, permeabilized and stained with either CA9Ab-680 or CA12Ab-680 in combination with a nuclear stain (DAPI) and a cell membrane marker (WGA). The ICC results were largely in agreement with the prior qRT-PCR results: CAIX levels were highly elevated in hypoxia relative to normoxia in all of the cell lines (Fig. 2a), whereas CAXII expression was highly elevated in hypoxia relative to normoxia only in MCF-10A cells and only slightly elevated in ZR-75.1 cells (Fig. 2b). As with the mRNA results, MCF-7 cells had high constitutive CAXII expression in normoxia. The constitutive (normoxic) CAXII expression was lower in DCIS cells than would have been predicted by mRNA. Therefore, mRNA levels were generally predictive of protein levels but the two measurements were not precisely associated.

### Ex vivo Analysis of Hypoxia-related CAIX and CAXII Expression

To evaluate CAIX and CAXII expression levels in hypoxic tumor regions, we generated mammary fat pad tumor xenografts using MDA-mb-231 cells which had increased CAIX expression but not CAXII in hypoxia *in vitro*; and ZR-75.1 cells which had increased expression of both markers in hypoxia *in vitro*. Tumors were harvested following administration of pimonidazole, a known hypoxia marker [40], and the CAIX and CAXII IHC staining, and pimonidazole staining patterns were evaluated regionally in center sections of the tumors. CAIX, CAXII and pimonidazole staining intensities and spatial distances from regions of necrosis were quantified pixel-by-pixel (Fig. 3). In both tumor types, pimonidazole staining was observed out to 600 μm from the edge of necrosis, with the highest staining occurring closer to the edge of necrosis, which strongly suggests hypoxic conditions in the tumor regions adjacent to necrosis. Similar to pimonidazole staining, both CAIX and CAXII had elevated IHC staining in the 600 μm adjacent to necrosis in both tumor types (Fig. 3a, b), albeit CAXII staining was much weaker relative to CAIX. CAIX staining was observed to a distance of 1,300 μm from the edge of necrosis indicating a persistence of expression beyond the limits of pimonidazole staining. Interestingly, in MDA-mb-231 tumors (Fig. 3b), CAXII staining was not detectable past 600 μm from the edge of necrosis, similar to pimonidazole staining. But for ZR-75.1 tumors, CAXII staining remained elevated out to 1,900 μm from necrosis.

### In vivo Correlation of Probe-related Fluorescence, Marker Expression and Hypoxia

Since ZR-75.1 cells demonstrated elevated mRNA (Fig. 1) and protein (Fig. 2) for both CAIX and CAXII when cultured in hypoxic conditions relative to normoxia, and elevated

expression of both markers in hypoxic tumor regions adjacent to necrosis (Fig. 3), this tumor line was selected to evaluate our NIRF probes *in vivo*. However, constitutive expression of both CAIX and CAXII were observed in ZR-75.1 cells *in vitro* (Fig. 2), *i.e.*, expression in normoxia. In order to better distinguish marker expression related to hypoxia non-invasively and *in vivo* by fluorescence imaging using our CA targeted fluorescent probes, mice were housed in varied levels of $O_2$. For comparison, the commercially available sulfonamide-based HypoxiSense 680 probe (Perkin-Elmer) that is generally specific for the carbonic anhydrase active site but is not isoform specific was also administered to the same treatment groups.

Three (n=8 each) groups of animals bearing ZR-75.1 xenograft MFP tumor were studied: (1) placed in a hypoxia induction chamber for 2 h; (2) in a hyperoxic induction chamber for 2 h; and (3) in normoxic conditions (open air). Each group was divided into two sub-groups ($n$=4 each) and either CA9Ab-680 or CA12Ab-680 was i.v. injected into each sub-group. Following injection, animals were quickly returned to hypoxic, hyperoxic or normoxic conditions for an additional 5 h. Then each animal was administered pimonidazole, returned to their respective chambers for an additional 30 min and imaged using the Optix MX3 imaging system (ART, Inc., Montreal, CA). Normalized fluorescence values were quantified for each group of animals (Fig. 4a). After imaging, tumors were excised and IHC stained to determine CAIX and CAXII expression and pimonidazole for hypoxia levels. Slides were scanned and staining intensities determined.

CA9Ab-680 normalized *in vivo* fluorescence values (Fig. 4a, left), CAIX IHC staining (Fig. 4b, left) and pimonidazole staining (Fig. 4c) decreased stepwise from hypoxic-to-normoxic-to-hyperoxic conditions. When comparing these decreases pairwise by Student's *t* test, normoxia-to-hypoxia and normoxia-to-hyperoxia, all changes were significant ($p$<0.025) except for normoxia to hyperoxia for IHC staining ($p$=0.06). By one-way ANOVA, the values for all three conditions were significantly different ($p$<0.001) for fluorescence, IHC and pimonidazole staining (Table 1). The Tukey-Cramer 95 % simultaneous confidence intervals were significant for all pairings except when comparing hypoxia to normoxia by CAIX IHC staining (Table 2).

Notably, CAXII-related fluorescence and IHC staining values were generally lower than CAIX and were not significantly altered among the three groups of animals as determined by pairwise Student's *t* test, one-way ANOVA and Tukey-Cramer confidence intervals (Fig. 4a, b, middle and Tables 1 and 2).

For the sulfonamide-based probe, which should specifically bind to both markers, the observed differences among the three groups were not statistically significant due to increased variability within each group (Fig. 4a, right and Tables 1 and 2). The image intensity values for the sulfonamide probe were higher and comparable to the CAIX and CAXII fluorescence values combined.

For CAIX, these *in vivo* results are in agreement with the *in vitro* and *ex vivo* results from this study, where for ZR-75.1 cells and tumors, CAIX expression was significantly induced by hypoxic conditions. For CAXII, these results were not necessarily inconsistent with the *in*

*vitro* results, where increased CA12Ab-680 probe uptake in hypoxia was only modestly increased from constitutive levels in ZR-75.1 cells *in vitro* (Fig. 2), and CAXII staining was only marginally elevated in hypoxic regions adjacent to necrosis (Fig. 3a).

An overlay of the CAIX and pimonidazole staining for a representative tumor section shows a strong association of CAIX-related fluorescence with pimonidazole-related fluorescence. However, CAIX fluorescence is also observed beyond the limits of pimonidazole staining, particularly at the outer tumor edge (Fig. 5a). Fluorescence micrographs were also generated at higher magnification to determine colocalization at the cellular level of blood perfusion (Hoechst stain), hypoxia (pimonidazole) and CA9Ab-680 or CA12Ab-680 fluorescence (Fig. 5b). In agreement with the macroscopic quantifications, CA9Ab-680 and CA12Ab-680 fluorescence co-localized with pimonidazole stained cells but also had staining that did not correspond to pimonidazole staining. Pimonidazole-associated fluorescence was spatially correlated with CAIX- and CAXII-associated fluorescence using pixel-by-pixel binning distribution analyses shown plotted in Fig. 5c. As can be seen in the plots, nearly all pimonidazole staining correlated with some CAIX or CAXII staining (center sector), whereas practically no pimonidazole staining is seen in the absence of CA staining (lower sector), but in both cases (CAIX and CAXII) there was some staining observed in the absence of pimonidazole (upper sector). The overlap coefficients generated by these analyses indicate a high correlation of CA expression with pimonidazole deposition (CA9Ab-680 overlap coefficient=0.88 and CA12Ab-680 overlap coefficient=0.82). However, in all cases (IHC and fluorescence) CAXII staining was weaker than CAIX staining. Hence, these results were consistent with those for ZR-75.1 cells and tumors throughout the study presented herein.

Time-domain fluorescence tomography was used to generate a slice-by-slice map of CA9Ab-680 fluorescence throughout a ZR-75.1 xenograft tumor in a living mouse (Fig. 6a). Heterogeneity of CA9Ab-680-related fluorescence was observed throughout the tumor, consistent with regions of hypoxia and normoxia (Fig. 6b). The *ex vivo* center section, along with H&E, CAIX and pimonidazole staining of adjacent sections are shown in Fig. 6c. The brightest fluorescence signal aligned with the region of darkest CAIX IHC staining, which co-registered with the pimonidazole staining, indicating a relationship between CAIX expression and hypoxia.

## Discussion

Our first aim in this study was the verification of CAIX and CAXII expression as markers for detection of hypoxia. Therefore, comparative analyses of the combined expression of these genes and proteins were performed in cell lines and breast tumor xenografts in the context of normoxia and hypoxia. According to our mRNA and protein determinations in breast cancer cell lines, CAIX expression was up-regulated in hypoxia to some degree in every breast cell line, regardless of some constitutive expression in normoxic conditions. However, CAXII expression was induced by hypoxia in some cell lines (*e.g.*, MCF-10A) with constitutive expression in normoxia observed for every line. Similar results have been reported by other groups, where the expression of *CA9* and *CA12* mRNA were analyzed in several cell lines derived from different tissue types and the amplitude of induction by

hypoxia was high for *CA9* in all the cell lines, while differential induction of *CA12* was also observed [16, 26, 41].

CAIX and CAXII IHC staining and pimonidazole staining of MDA-mb-231 and ZR-75.1 xenografts revealed that both markers have elevated expression in tumor regions adjacent to necrosis and that these regions are hypoxic. In both tumor types, CAIX staining extended farther from necrosis compared to pimonidazole staining. This could be due to the relative oxygenation thresholds of pimonidazole staining compared to CAIX expression induction, *i.e.*, the threshold for pimonidazole staining is <1.3 % oxygen, whereas upregulation of molecular markers such as CAIX occur at pO2 values over a larger range, 0.2–2 % oxygen [42]; or this expression further from necrosis could alternatively be a result of short-lived fluctuations in tumor perfusion combined with slow rates of CAIX degradation [43], *i.e.*, transient (acute) hypoxia; or this expression could be related to constitutive expression of the marker in normoxic conditions, as was observed in the ICC staining of ZR-75.1 cells for CAIX (Fig. 2). This incomplete registration of CAIX expression with pimonidazole staining has also been reported by other groups [12, 41–44]. For CAXII, IHC staining was co-localized with pimonidazole staining in MDA-mb-231 tumors. However, in ZR-75.1 tumors, CAXII staining was observed to extend farther from necrosis relative to pimonidazole, similar to CAIX staining in both tumor types. Interestingly, the CAXII expression pattern in the tumors did not perfectly match the ICC results, where the MDA-mb-231 ICC showed relatively high expression in normoxia, but the tumor expression highly corresponded with pimonidazole staining. Other groups have also reported focal induction of CAXII in areas adjacent to necrosis [23, 25], but that CAXII expression is less predictable compared to CAIX [25, 45].

To investigate how probe retention and accumulation in tumor is related to marker expression and hypoxia, we further studied ZR-75.1 tumor-bearing animals housed in hypoxic, normoxic and hyperoxic conditions and demonstrated that the accumulation of CA9Ab-680-related fluorescence and CAIX expression are both increased in a hypoxia-dependent manner. Hypoxia-induced accumulation and induction was not observed for CA12Ab-680 or CAXII respectively. This result is not necessarily in conflict with the *in vitro* studies that show CAXII induction by hypoxia in ZR-75.1 cells and increased CAXII in ZR-75.1 tumors at the necrotic interface in *ex vivo* studies as the observed induction was only marginally higher than the constitutive CAXII expression observed in tumor cells farther away from the necrosis (Fig. 3a), possibly making induction of CAXII expression in hypoxia not detectable above background in this model by *in vivo* imaging. The combination treatment used in this study has been shown to reduce tumor hypoxia in pre-clinical [44] and clinical [36] settings, and pimonidazole staining was used herein to confirm the level of hypoxia present in tumors of each treatment group. We have also done the same study for a sulfonamide-based NIRF probe (HypoxiSense 680) to test whether sulfonamide-based probes that detect both CAIX and CAXII by targeting the CA active site are capable of detecting hypoxia. Our results with the sulfonamide probe showed a trend, but no significant difference, among the treatment groups. This could be due to the lack of substrate specificity for CAIX, *i.e.*, sulfonamides are also avid for CAXII as the image intensity values for the sulfonamide probe were comparable to the addition of the CAIX and CAXII specific

signals. Therefore, imaging probes that specifically target CAIX may provide superior results compared to probes that non-specifically target the CA active site and can cross-react with expression of other cell-surface CA isoforms, *e.g.*, CAXII.

The results of fluorescence images and micrographs acquired from ZR-75.1 tumor sections revealed that both CAIX and CAXII expression nearly completely overlap with the regions of hypoxia (pimonidazole staining), but are also present in perfused areas without pimonidazole staining, including strong staining of CAIX at the tumor periphery (Fig. 5a). High CAIX expression at the edge of the tumors could be related to the development of an invasive phenotype of cells in this region [45]. It has been proposed that CAIX activity may participate in acidification of the extracellular microenvironment [46]. Hence, some tumors appear to have a baseline level of constitutive CAIX expression that is not related to hypoxia induction and that could be involved in tumor cell invasion at the tumor periphery.

Our study revealed mixed results for CAXII, where all of the breast cell lines tested had a baseline level of constitutive expression, but only a subset of the cells had additional expression induced by hypoxia. The mechanism of hypoxia-related induction of CAXII expression is not known; however, there is some evidence of a differentiation related mechanism. A recent study demonstrated that the *CA12* gene, and not *CA9*, is regulated *via* the estrogen receptor A in breast cancer cells, and that this regulation involves a distal estrogen-responsive enhancer region [49].

## Conclusion

We have shown that CAIX but not CAXII is a reliable surrogate marker of hypoxia in breast cancer. Although CAIX expression may be observed in areas throughout the tumor regardless of hypoxia, it was consistently up-regulated in regions of hypoxia and by induction of hypoxia. Hence, CAIX has greater potential for use as an imaging biomarker of hypoxia. However, this study implies that caution should be taken when using agents that target the carbonic anhydrase active site as hypoxia surrogates in breast cancer, *e.g.*, sulfonamide-based imaging probes [47], as CAXII expression was constitutively elevated in a number of the breast tumors surveyed. Therefore, CAIX-specific imaging agents such as CA9Ab-680 for fluorescence, $^{111}$In-ITC-DTPA-cG250 for SPECT [48] and $^{124}$I-cG250 [31] for PET have potential for non-invasive hypoxia assessment. There is also potential for use of a CAIX-specific imaging agent to follow alterations in CAIX expression as an indicator of treatment response in a wide range of tumors. Antibody-based agents have the advantage of high specificity, but due to their large molecular size, these agents have long circulation times and slow rates of tumor accumulation and clearance from the body. Therefore, development of a smaller, high affinity and high specificity CAIX targeting agents (*e.g.*, peptides) are needed.

## Acknowledgments

The authors wish to acknowledge the following core facilities at the H. Lee Moffitt Cancer Center & Research Institute for their contributions to this work: Analytic Microscopy, Tissue, Molecular Genomics, Comparative Biomedicine and the Small Animal Imaging Laboratory. This work was supported in part by the Cancer Center Support Grant P30 CA076292 from the National Cancer Institute. NIH Grant Support: NIH/NCI R01CA077575 (RJG).

## Abbreviations

| | |
|---|---|
| **CAIX** | Carbonic anhydrase IX |
| **CAXII** | Carbonic anhydrase XII |

## References


1. Gatenby RA, Gillies RJ. Why do cancers have high aerobic glycolysis? Nat Rev Cancer. 2004; 4:891–899. [PubMed: 15516961]
2. Cairns RA, Papandreou I, Sutphin PD, Denko NC. Metabolic targeting of hypoxia and HIF1 in solid tumors can enhance cytotoxic chemotherapy. Proc Natl Acad Sci U S A. 2007; 104:9445–9450. [PubMed: 17517659]
3. Wojtkowiak JW, Cornnell HC, Matsumoto S, et al. Pyruvate sensitizes pancreatic tumors to hypoxia-activated prodrug TH-302. Cancer Metabol. 2015; 3:2.
4. Wouters A, Pauwels B, Lardon F, Vermorken JB. Review: implications of *in vitro* research on the effect of radiotherapy and chemotherapy under hypoxic conditions. Oncologist. 2007; 12:690–712. [PubMed: 17602059]
5. Harris AL. Hypoxia—a key regulatory factor in tumour growth. Nat Rev Cancer. 2002; 2:38–47. [PubMed: 11902584]
6. Kaanders JH, Wijffels KI, Marres HA, et al. Pimonidazole binding and tumor vascularity predict for treatment outcome in head and neck cancer. Cancer Res. 2002; 62:7066–7074. [PubMed: 12460928]
7. Sun JD, Liu Q, Wang J, et al. Selective tumor hypoxia targeting by hypoxia-activated prodrug TH-302 inhibits tumor growth in preclinical models of cancer. Clin Cancer Res. 2012; 18:758–770. [PubMed: 22184053]
8. Evans SM, Koch CJ. Prognostic significance of tumor oxygenation in humans. Cancer Lett. 2003; 195:1–16. [PubMed: 12767506]
9. Sun X, Niu G, Chan N, et al. Tumor hypoxia imaging. Mol Imaging Biol. 2011; 13:399–410. [PubMed: 20838906]
10. Gatenby RA, Kessler HB, Rosenblum JS, et al. Oxygen distribution in squamous cell carcinoma metastases and its relationship to outcome of radiation therapy. Int J Radiat Oncol Biol Phys. 1988; 14:831–838. [PubMed: 3360652]
11. Nozue M, Lee I, Yuan F, et al. Interlaboratory variation in oxygen tension measurement by Eppendorf “Histograph” and comparison with hypoxic marker. J Surg Oncol. 1997; 66:30–38. [PubMed: 9290690]
12. Jenkins WT, Evans SM, Koch CJ. Hypoxia and necrosis in rat 9L glioma and Morris 7777 hepatoma tumors: comparative measurements using EF5 binding and the Eppendorf needle electrode. Int J Radiat Oncol Biol Phys. 2000; 46:1005–1017. [PubMed: 10705024]
13. He F, Deng X, Wen B, et al. Noninvasive molecular imaging of hypoxia in human xenografts: comparing hypoxia-induced gene expression with endogenous and exogenous hypoxia markers. Cancer Res. 2008; 68:8597–8606. [PubMed: 18922936]
14. Bussink J, Kaanders JH, van der Kogel AJ. Tumor hypoxia at the micro-regional level: clinical relevance and predictive value of exogenous and endogenous hypoxic cell markers. Radiother Oncol. 2003; 67:3–15. [PubMed: 12758235]
15. Olive PL, Aquino-Parsons C, MacPhail SH, et al. Carbonic anhydrase 9 as an endogenous marker for hypoxic cells in cervical cancer. Cancer Res. 2001; 61:8924–8929. [PubMed: 11751418]
16. Wykoff CC, Beasley NJ, Watson PH, et al. Hypoxia-inducible expression of tumor-associated carbonic anhydrases. Cancer Res. 2000; 60:7075–7083. [PubMed: 11156414]
17. Koch CJ, Evans SM, Lord EM. Oxygen dependence of cellular uptake of EF5 [2-(2-nitro-1H-imidazol-1-yl)-N-(2,2,3,3,3-pentafluoropropyl)a cet amide] : analysis of drug adducts by fluorescent antibodies vs bound radioactivity. Br J Cancer. 1995; 72:869–874. [PubMed: 7547233]

18. Raleigh JA, Calkins-Adams DP, Rinker LH, et al. Hypoxia and vascular endothelial growth factor expression in human squamous cell carcinomas using pimonidazole as a hypoxia marker. Cancer Res. 1998; 58:3765–3768. [PubMed: 9731480]
19. Mees G, Dierckx R, Vangestel C, Van de Wiele C. Molecular imaging of hypoxia with radiolabelled agents. Eur J Nucl Med Mol Imaging. 2009; 36:1674–1686. [PubMed: 19565239]
20. Cook GJ. Oncological molecular imaging: nuclear medicine techniques. Br J Radiol. 2003; 76(Spec No 2):S152–S158. [PubMed: 15572337]
21. Pastorekova S, Zatovicova M, Pastorek J. Cancer-associated carbonic anhydrases and their inhibition. Curr Pharm Des. 2008; 14:685–698. [PubMed: 18336315]
22. Chi JT, Wang Z, Nuyten DS, et al. Gene expression programs in response to hypoxia: cell type specificity and prognostic significance in human cancers. PLoS Med. 2006; 3:e47. [PubMed: 16417408]
23. Winum JY, Scozzafava A, Montero JL, Supuran CT. Inhibition of carbonic anhydrase IX: a new strategy against cancer. Anti cancer Agents Med Chem. 2009; 9:693–702.
24. Zatovicova M, Jelenska L, Hulikova A, et al. Carbonic anhydrase IX as an anticancer therapy target: preclinical evaluation of internalizing monoclonal antibody directed to catalytic domain. Curr Pharm Des. 2010; 16:3255–3263. [PubMed: 20819068]
25. Supuran CT, Scozzafava A. Carbonic anhydrases as targets for medicinal chemistry. Bioorg Med Chem. 2007; 15:4336–4350. [PubMed: 17475500]
26. Ivanov S, Liao SY, Ivanova A, et al. Expression of hypoxia-inducible cell-surface transmembrane carbonic anhydrases in human cancer. Am J Pathol. 2001; 158:905–919. [PubMed: 11238039]
27. Tafreshi NK, Bui MM, Bishop K, et al. Noninvasive detection of breast cancer lymph node metastasis using carbonic anhydrases IX and XII targeted imaging probes. Clin Cancer Res. 2012; 18:207–219. [PubMed: 22016510]
28. Watson PH, Chia SK, Wykoff CC, et al. Carbonic anhydrase XII is a marker of good prognosis in invasive breast carcinoma. Br J Cancer. 2003; 88:1065–1070. [PubMed: 12671706]
29. Ivanov SV, Kuzmin I, Wei MH, et al. Down-regulation of transmembrane carbonic anhydrases in renal cell carcinoma cell lines by wild-type von Hippel-Lindau transgenes. Proc Natl Acad Sci U S A. 1998; 95:12596–12601. [PubMed: 9770531]
30. Pastorekova S, Parkkila S, Zavada J. Tumor-associated carbonic anhydrases and their clinical significance. Adv Clin Chem. 2006; 42:167–216. [PubMed: 17131627]
31. Bahnson EE, Murrey DA, Mojzisik CM, et al. PET/CT imaging of clear cell renal cell carcinoma with I labeled chimeric antibody. Ther Adv Urol. 2009; 1:67–70. [PubMed: 21789055]
32. Divgi CR, Pandit-Taskar N, Jungbluth AA, et al. Preoperative characterisation of clear-cell renal carcinoma using iodine-124-labelled antibody chimeric G250 (124I-cG250) and PET in patients with renal masses: a phase I trial. Lancet Oncol. 2007; 8:304–310. [PubMed: 17395103]
33. Dubois L, Lieuwes NG, Maresca A, et al. Imaging of CA IX with fluorescent labelled sulfonamides distinguishes hypoxic and (re)-oxygenated cells in a xenograft tumour model. Radiother Oncol. 2009; 92:423–428. [PubMed: 19616332]
34. Barathova M, Takacova M, Holotnakova T, et al. Alternative splicing variant of the hypoxia marker carbonic anhydrase IX expressed independently of hypoxia and tumour phenotype. Br J Cancer. 2008; 98:129–136. [PubMed: 18026188]
35. Morse DL, Carroll D, Weberg L, et al. Determining suitable internal standards for mRNA quantification of increasing cancer progression in human breast cells by real-time reverse transcriptase polymerase chain reaction. Anal Biochem. 2005; 342:69–77. [PubMed: 15958182]
36. Kaanders JH, Pop LA, Marres HA, et al. Accelerated radiotherapy with carbogen and nicotinamide (ARCON) for laryngeal cancer. Radiother Oncol. 1998; 48:115–122. [PubMed: 9783882]
37. Kumar AT, Raymond SB, Dunn AK, et al. A time domain fluorescence tomography system for small animal imaging. IEEE Trans Med Imaging. 2008; 27:1152–1163. [PubMed: 18672432]
38. Kim J. The computation of bivariate normal and t probabilities, with application to comparisons of three normal means. Comput Stat Data Anal. 2013; 58:177–186.
39. Tafreshi NK, Enkemann SA, Bui MM, et al. A mammaglobin—a targeting agent for noninvasive detection of breast cancer metastasis in lymph nodes. Cancer Res. 2011; 71:1050–1059. [PubMed: 21169406]

40. Varia MA, Calkins-Adams DP, Rinker LH, et al. Pimonidazole: a novel hypoxia marker for complementary study of tumor hypoxia and cell proliferation in cervical carcinoma. Gynecol Oncol. 1998; 71:270–277. [PubMed: 9826471]

41. Chiche J, Ilc K, Laferriere J, et al. Hypoxia-inducible carbonic anhydrase IX and XII promote tumor cell growth by counteracting acidosis through the regulation of the intracellular pH. Cancer Res. 2009; 69:358–368. [PubMed: 19118021]

42. Beasley NJ, Wykoff CC, Watson PH, et al. Carbonic anhydrase IX, an endogenous hypoxia marker, expression in head and neck squamous cell carcinoma and its relationship to hypoxia, necrosis, and microvessel density. Cancer Res. 2001; 61:5262–5267. [PubMed: 11431368]

43. Carlin S, Khan N, Ku T, et al. Molecular targeting of carbonic anhydrase IX in mice with hypoxic HT29 colorectal tumor xenografts. PLoS One. 2010; 5:e10857. [PubMed: 20523727]

44. van Laarhoven HW, Bussink J, Lok J, et al. Effects of nicotinamide and carbogen in different murine colon carcinomas: immunohistochemical analysis of vascular architecture and micro-environmental parameters. Int J Radiat Oncol Biol Phys. 2004; 60:310–321. [PubMed: 15337570]

45. Onogawa S, Kitadai Y, Tanaka S, et al. Expression of VEGF-C and VEGF-D at the invasive edge correlates with lymph node metastasis and prognosis of patients with colorectal carcinoma. Cancer Sci. 2004; 95:32–39. [PubMed: 14720324]

46. Svastova E, Hulikova A, Rafajova M, et al. Hypoxia activates the capacity of tumor-associated carbonic anhydrase IX to acidify extracellular pH. FEBS Lett. 2004; 577:439–445. [PubMed: 15556624]

47. Supuran CT. Carbonic anhydrases: novel therapeutic applications for inhibitors and activators. Nat Rev Drug Discov. 2008; 7:168–181. [PubMed: 18167490]

48. Brouwers AH, Buijs WC, Oosterwijk E, et al. Targeting of metastatic renal cell carcinoma with the chimeric monoclonal antibody G250 labeled with (131)I or (111) In: an intrapatient comparison. Clin Cancer Res. 2003; 9:3953S–3960S. [PubMed: 14506194]

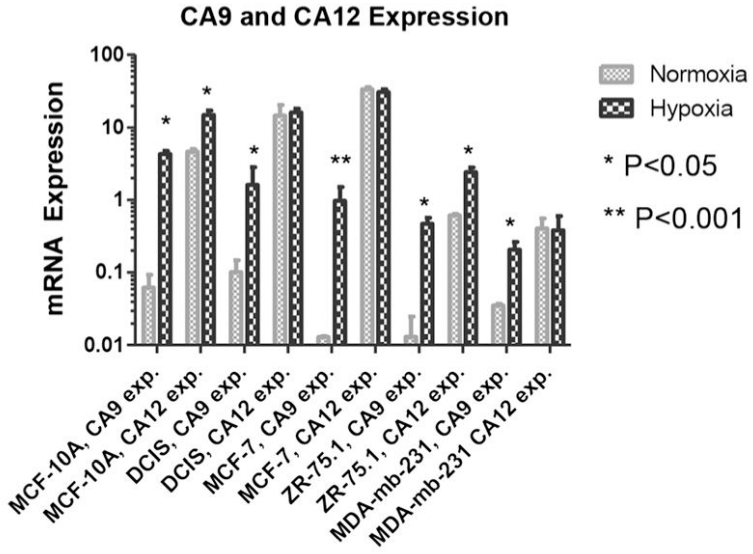


**Fig. 1.**

mRNA expression, ($2^{-CT\ gene}$ /$2^{-CT\ \beta\text{-actin}}$)* 1,000, of *CA9* and *CA12* in MCF-10A, DCIS, MCF-7, ZR-75.1 and MDA-mb-231 breast cancer cells in normoxic and hypoxic conditions. Cells were grown under either normal oxygen conditions (20 %) or limiting oxygen conditions (<2 %) for approximately 16 h prior to mRNA extraction and qRT-PCR. Data are represented as mean±S.D. Note the Log 10 scale. Significant *p* values, normoxia compared to hypoxia, are indicated by *asterisks*.

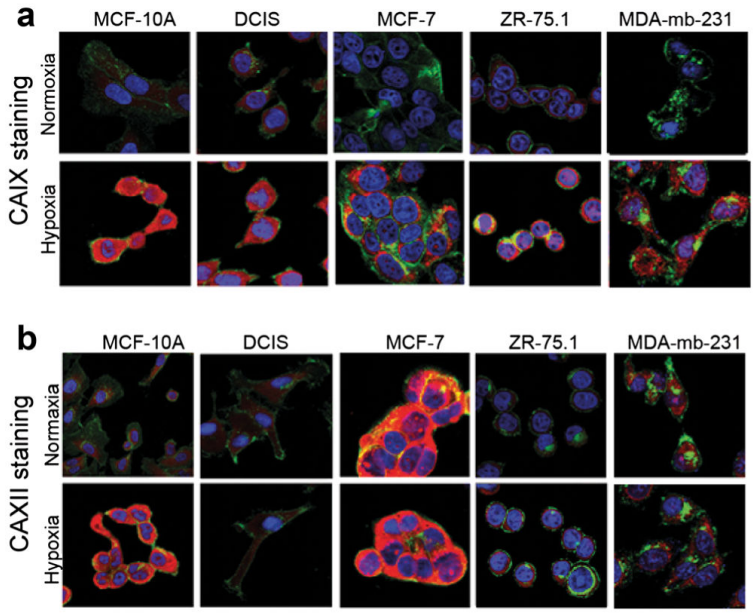


**Fig. 2.**

**a** and **b** ICC staining of breast cancer cells incubated in normoxic and hypoxic conditions using the CA9Ab-680 and CA12Ab-680 probes. Confocal micrographs of cells incubated with the nuclear marker DAPI (*blue*), the plasma- and cytoplasmic-membrane marker, WGA (*green*) and CA9Ab-680 or CA12Ab-680 (*red*). **a** Stronger CA9Ab-680 staining is observed for all breast cancer cell lines grown in hypoxia relative to normoxia. **b** Hypoxia-induced CA12Ab-680 staining is observed in MCF-10A and ZR-75.1 cells, and comparable levels of constitutive expression in normoxia and hypoxia are observed in DCIS, MCF-7 and MDA-mb-231 cells. Cytoplasmic staining is observed due to permeabilization of cells after fixation.

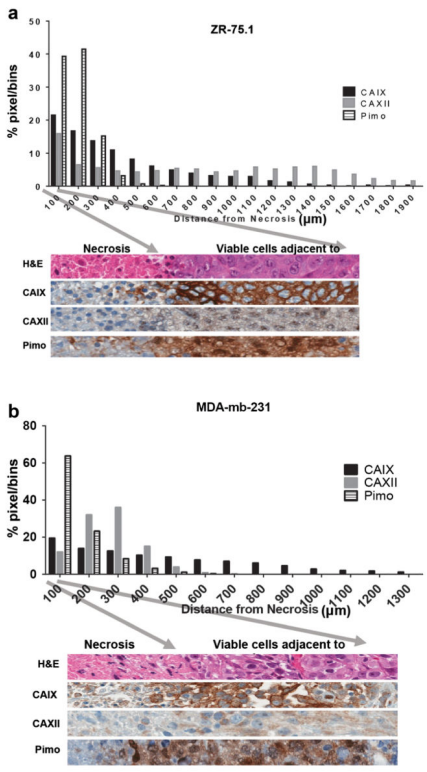


**Fig. 3.**

Regional relative (normalized) expression of CAIX and CAXII protein in breast cancer xenograft tumors by quantitative image analysis of IHC and pimonidazole stained tumor sections. Protein staining intensities of **a** ZR-75.1 and **b** MDA-mb-231 tumors graphed by distance from necrosis. Representative images are shown from each tumor xenograft below each graph. The *arrows* correspond to the tumor/necrotic edge (*left arrow*) and the bin limit of 100 pixels. Please note that thresholds for strong positive stained tumor tissue varied between stains. The strong positive threshold for CAIX was set much higher than the threshold for CAXII. This was due to the intrinsic expression differences and was held constant for these experiments.

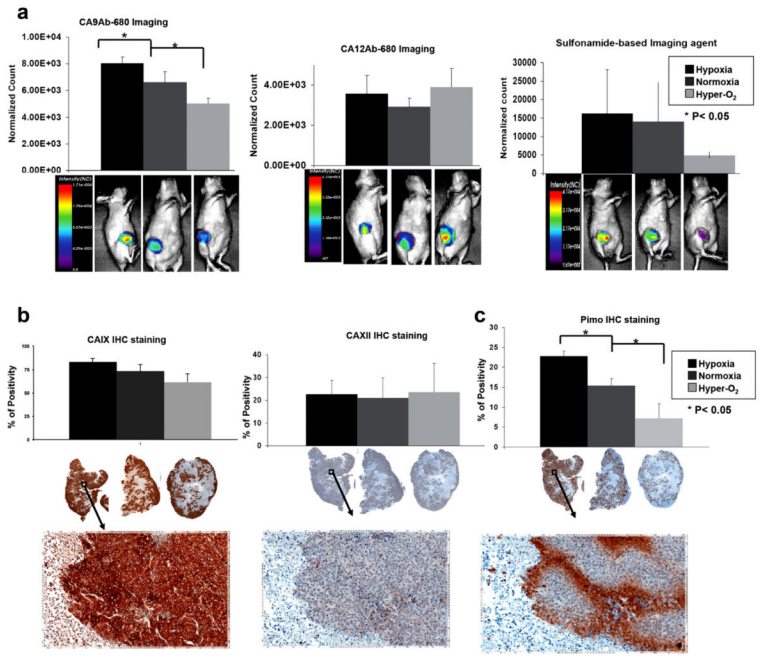


**Fig. 4.**

*In vivo* expression of CAIX and CAXII in hypoxic, normoxic and hyperoxic conditions. **a** Quantification of CA9Ab-680, CA12Ab-680 and HypoxiSense680 (a sulfonamide-based probe from Perkin-Elmer)-related fluorescence in ZR-75.1 tumors of animals treated with 7 % oxygen (hypoxia, *black*), no treatment (normoxia, dark *gray*), or nicotinamide and carbogen (hyper-$O_2$, *light gray*). Representative images are shown from each group of animals below each graph. Note that the scales are different and the images were acquired 5 h after agent administration. **b** Quantification of CAIX and CAXII IHC staining of ZR-75.1 tumors from the same animals presented in panel Images of representative IHC staining are underneath each graph. **c** Quantification of pimonidazole staining (hypoxia marker) for the same set of animals presented above with representative of low and high magnification images of staining underneath each graph. Data represent the mean±SD of at least four independent animals. *Asterisk* indicates significant difference (*$p$<0.05) compared to no treatment.

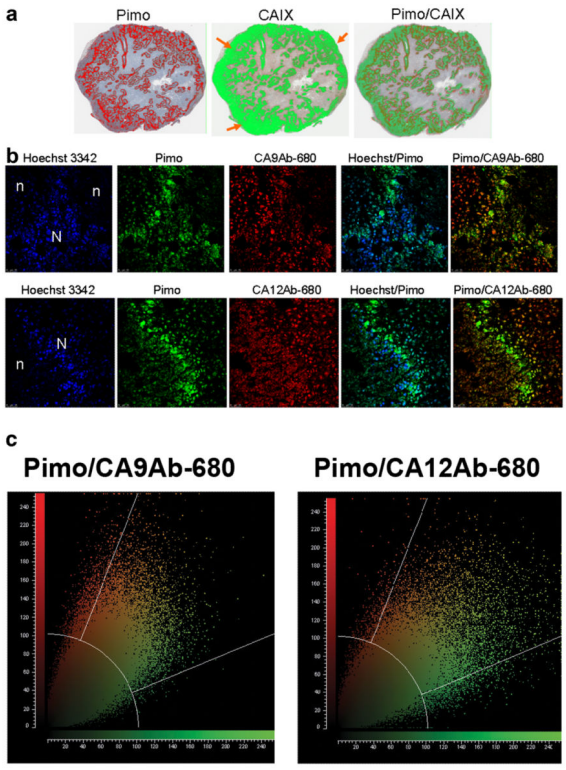


**Fig. 5.**

**a** Masked representation of pimonidazole (*red*) and CAIX (*green*) staining of a representative ZR-75.1 tumor from an animal housed in hypoxic conditions. The *far right panel* is an overlay of staining for the two markers (*yellow*: overlay of CAIX and Pimo). Note the strong staining of CAIX at the edge of the tumors indicated by *orange arrows*. **b** Fluorescence confocal micrographs of ZR-75.1 tumor sections. Tumors were removed 24 h post intravenous injection of CA9Ab-680 or CA12Ab-680 probe. Pimonidazole was injected 30 min before euthanasia. Hoechst 3342 dye was injected 1 min before euthanasia for tumor cell morphology; *n*=regions of necrosis and *N*=normal. **c** Pixel-by-pixel binning distribution analyses of pimonidazole staining (*green*) and CA9Ab-680 (*red, top panel*) and CA12Ab-680 staining (*red, bottom panel*). *Yellow color* shows co-registration of pixels. CA9Ab-680 overlap coefficient=0.88 and CA12Ab-680 overlap coefficient=0.82.

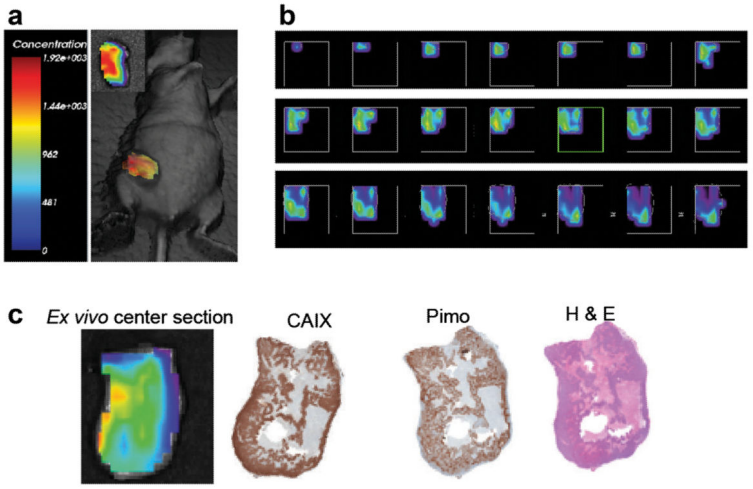


**Fig. 6.**

Fluorescence tomographic imaging of ZR-75.1 xenograft tumor. **a** 3D reconstruction of CA9Ab-680 fluorescence in a ZR-75.1 tumors 5 h post administration of probe. *Inset* shows *ex vivo* image of the whole tumor. **b** Top to bottom slices of the same tumor. Slices are 1 mm thick each, ranging from the upper left (top of tumor) to the lower right (bottom of tumor). **c** From left to right, *ex vivo* fluorescence image of a 1 mm center section of the tumor and corresponding CAIX IHC staining, pimonidazole staining and H&E staining of adjacent sections taken from the 1-mm center section. The 1-mm center section was cut in the coronal orientation in order to register with the tomographic image as best possible.

**Table 1**

One-way ANOVA analysis results

| Item | | Hypoxia | Normoxia | Hyper-$O_2$ | MSE | *p* value |
|---|---|---|---|---|---|---|
| CAIX IHC staining | Mean | 0.84 | 0.74 | 0.62 | 0.0048 | <0.001 |
| | *n* | 8 | 4 | 6 | | |
| CA9Ab680 fluorescence | Mean | 8,055 | 6,620 | 5,035 | 290,900 | <0.001 |
| | *n* | 4 | 3 | 4 | | |
| CAXII IHC staining | Mean | 0.23 | 0.21 | 0.24 | 0.0092 | 0.88 |
| | *n* | 8 | 5 | 8 | | |
| CA12Ab680 fluorescence | Mean | 3566.7 | 2920.0 | 3895.0 | 654,881 | 0.32 |
| | *n* | 3 | 3 | 4 | | |
| HypoxiSense 680 | Mean | 16,300 | 14,000 | 4,960 | | 0.35 |
| | *n* | 3 | 3 | 3 | | |
| Pimonidazole staining | Mean | 23.6 | 15.4 | 7.2 | 5.97 | <0.001 |
| | *n* | 4 | 4 | 4 | | |

The *p* value was computed by the method by Kim [38].

*MSE* mean square error

## Table 2

The Tukey-Cramer 95 % simultaneous confidence interval

| Item | Arm Comparisons | Lower | Upper | Note |
|---|---|---|---|---|
| CAIX IHC staining | Hypoxia - Normoxia | −0.006 | 0.21 | Not Significant |
| | Normoxia - Hyper-$O_2$ | 0.002 | 0.23 | Significant |
| | Hypoxia - Hyper-$O_2$ | 0.12 | 0.32 | Significant |
| CA9Ab680 fluorescence | Hypoxia - Normoxia | 259 | 2,612 | Significant |
| | Normoxia - Hyper-$O_2$ | 408 | 2,762 | Significant |
| | Hypoxia - Hyper-$O_2$ | 1,931 | 4,120 | Significant |
| CAXII IHC staining | Hypoxia - Normal | −0.12 | 0.16 | Not Significant |
| | Normal - Hyper $O_2$ | −0.17 | 0.11 | Not Significant |
| | Hypoxia - Hyper $O_2$ | −0.13 | 0.11 | Not Significant |
| CA12Ab680 fluorescence | Hypoxia - Normal | −1,299 | 2,592 | Not Significant |
| | Normal - Hyper $O_2$ | −2,795 | 845 | Not Significant |
| | Hypoxia - Hyper $O_2$ | −2,148 | 1,491 | Not Significant |
| HypoxiSense 680 | Hypoxia - Normal | −20,751 | 25,271 | Not Significant |
| | Normal - Hyper $O_2$ | −13,978 | 32,045 | Not Significant |
| | Hypoxia - Hyper $O_2$ | −11,718 | 34,305 | Not Significant |
| Pimonidazole staining | Hypoxia - Normoxia | 3.42 | 13.06 | Significant |
| | Normoxia - Hyper-$O_2$ | 3.39 | 13.03 | Significant |
| | Hypoxia - Hyper-$O_2$ | 11.7 | 21.3 | Significant |

The simultaneous confidence intervals were computed by using the critical point by Kim [38]. In CAIX IHC staining, the difference between Hypoxia and Normal is not significant